

## Article

# Synthesis of Photoluminescent Carbon Dots Using *Hibiscus* Tea Waste and Heteroatom Doping for Multi-Metal Ion Sensing: Applications in Cell imaging and Environmental Samples

Sonaimuthu Mohandoss <sup>1,†</sup>, Naushad Ahmad <sup>2,\*</sup> , Kuppu Sakthi Velu <sup>1,†</sup>, Mohammad Rizwan Khan <sup>2</sup> , Subramanian Palanisamy <sup>3</sup> , SangGuan You <sup>3</sup> and Yong Rok Lee <sup>1,\*</sup>

<sup>1</sup> School of Chemical Engineering, Yeungnam University, Gyeongsan 38541, Republic of Korea; drsmohandoss@yu.ac.kr (S.M.); sakthi.velu4@gmail.com (K.S.V.)

<sup>2</sup> Department of Chemistry, College of Science, King Saud University, Riyadh 11451, Saudi Arabia; mrkhan@ksu.edu.sa

<sup>3</sup> Department of Marine Food Science and Technology, Gangneung-Wonju National University, 120 Gangneungdaehangno, Gangneung 25457, Republic of Korea; spalanisamy33@gwnu.ac.kr (S.P.); umyousg@gwnu.ac.kr (S.Y.)

\* Correspondence: anaushad@ksu.edu.sa (N.A.); yrlee@yu.ac.kr (Y.R.L.)

† These authors contributed equally to this work.

**Abstract:** Novel photoluminescent carbon dots (CDs) were synthesized through a facile hydrothermal method using *Hibiscus* tea extract as a natural carbon source and boric acid as a boron source. The optical and physicochemical properties of the as-synthesized nitrogen- and boron-doped CDs (NB-CDs) were characterized using UV-Visible (UV-Vis), photoluminescence (PL) spectroscopy, Fourier-transform infrared (FTIR), X-ray diffraction (XRD), X-ray photoelectron spectroscopy (XPS), and transmission electron microscopy (TEM). The as-synthesized NB-CDs showed spherical morphology of approximately  $6.2 \pm 0.5$  nm with quantum yield (9.2%), high aqueous solubility, strong photostability, and excitation-dependent PL behavior. The obtained NB-CDs exhibited high stability over a wide pH range and high ionic strength. Additionally, NB-CDs exhibited PL enhancement response with excellent sensitivity toward multi-metal ions, including  $\text{Ag}^+$ ,  $\text{Cd}^{2+}$ , and  $\text{Cr}^{3+}$  ions, with very low detection limits of 44.5, 164.4, and 54.6 nM, respectively, with a wide concentration range of 0–10  $\mu\text{M}$ . Upon testing the cytotoxicity of the NB-CDs at a concentration of 20  $\mu\text{g}/\text{mL}$  for 24 h, we found no obvious inhibition of cell viability. Therefore, the proposed sensor method can be successfully applied to detect  $\text{Ag}^+$ ,  $\text{Cd}^{2+}$ , and  $\text{Cr}^{3+}$  ions in cell imaging as well as in real water environmental samples.

**Keywords:** carbon dots; photoluminescence; biomass; multi-metal ions; biological imaging; real samples



**Citation:** Mohandoss, S.; Ahmad, N.; Velu, K.S.; Khan, M.R.; Palanisamy, S.; You, S.; Lee, Y.R. Synthesis of Photoluminescent Carbon Dots Using *Hibiscus* Tea Waste and Heteroatom Doping for Multi-Metal Ion Sensing: Applications in Cell imaging and Environmental Samples. *Chemosensors* **2023**, *11*, 474. <https://doi.org/10.3390/chemosensors11090474>

Academic Editor: Lin Yuan

Received: 15 June 2023

Revised: 25 July 2023

Accepted: 7 August 2023

Published: 24 August 2023



**Copyright:** © 2023 by the authors. Licensee MDPI, Basel, Switzerland. This article is an open access article distributed under the terms and conditions of the Creative Commons Attribution (CC BY) license (<https://creativecommons.org/licenses/by/4.0/>).

## 1. Introduction

Detection of heavy metal ions in water samples is the most critical task in environmental analysis [1]. Food and water can be contaminated by ions such as  $\text{Ag}^+$ ,  $\text{Cd}^{2+}$ , and  $\text{Cr}^{3+}$  in the environment. Drinking water and fish farms are subject to strict limits on metal ions set by the World Health Organization (WHO) and Environmental Protection Agency (EPA) [2,3]. Numerous studies have reported that determining trace metal ions with high selectivity and sensitivity remains challenging [4]. To minimize human endangerment caused by heavy metal ions, a simple means of detection of heavy metal ions is crucial. Heavy metal ions are typically detected using colorimetric methods, atomic absorption spectrometry, ICP-MS, and fluorescence methods [5–8]. Nevertheless, the routine determination of  $\text{Ag}^+$ ,  $\text{Cd}^{2+}$ , and  $\text{Cr}^{3+}$  ions is limited by time-consuming, complicated methods

and costly equipment. The fluorescence method is one of the most widely used techniques owing to its sensitivity and simplicity [9,10]. This technique can detect heavy metal ions through biological and environmental analyses.

Nanomaterials are attracting increasing attention, particularly the synthesis of nanomaterials using waste biomass as a raw material. A new class of fluorescent nanomaterials, i.e., carbon dots (CDs), has emerged since 2006, showing interesting applications in sensing, bioimaging, catalysis, and drug delivery [11]. CDs are known for their photoluminescent properties owing to their ultra-small size, surface passivation, and unique optical and physicochemical properties [12]. Furthermore, CDs are water soluble, less toxic, chemically stable, and easily functionalized and exhibit superior biocompatibility [13]. However, it is important to adjust the microstructure of CDs to make them suitable for various applications. Doping affects the intrinsic properties of CDs, including their electronic properties and surface and chemical reactivity [14]. The electronic structure of crystals can be altered by introducing atomic impurities such as nitrogen (N), phosphorus (P), or boron (B). In recent years, researchers have increasingly focused on the controlled synthesis of heteroatom-doped CDs, especially those with nitrogen (N) and boron (B) doping [15–17]. Several methods are available for synthesizing photoluminescent N- and B-doped CDs (NB-CDs), including laser ablation, microwave irradiation, electrochemistry, ultrasound, and hydrothermal reactions [18]. Among these, hydrothermal methods are efficient, facile, and environmentally friendly.

Moreover, carbon materials can be produced from waste biomass, including soil waste such as ginkgo leaves, pineapple leaves, tea extract, mango peels, and banana peels [19–24], thereby reducing soil pollution and making the best use of resources. *Hibiscus sabdariffa* is one of the most commonly used ingredients in commercial herbal tea [25]. *H. sabdariffa* has been traditionally used in the food industry for herbal drinks or as a flavoring agent [26–28]. The hibiscus plant produces brightly colored flowers that are used to brew hibiscus tea [29]. Hibiscus blooms have five common colors: red, orange, pink, yellow, and white. Hibiscus plants have “calyxes”, which protect their blooms. Hibiscus tea is prepared using dried calyxes to impart a tart and refreshing taste. Hibiscus tea also contains trace minerals, including potassium, calcium, and magnesium [30]. Following various stages of tea processing, vast amounts of tea stalks and dust are removed, generating waste biomass [31]. Thus, owing to its high yield, low cost, biodegradability, and recyclability, hibiscus tea extract is ideal for the production of carbon materials [32].

Here, we described a method for synthesizing CDs from *Hibiscus* herbal tea extract using boric acid as a doping agent (Figure 1). We also demonstrated the application of the synthesized CDs as fluorescent probes for  $\text{Ag}^+$ ,  $\text{Cd}^{2+}$ , and  $\text{Cr}^{3+}$  ions. Various physicochemical techniques were used to characterize the NB-CDs, including UV–Vis, PL, FTIR, XRD, XPS, and TEM analysis. Strong green emission was observed from the synthesized NB-CDs, indicating their photoluminescence stability, high water solubility, and uniform size. Additionally, the NB-CDs were highly selective and sensitive for the detection of  $\text{Ag}^+$ ,  $\text{Cd}^{2+}$ , and  $\text{Cr}^{3+}$  ions, with limits of detection (LODs) of 44.5, 164.4, and 54.6 nM. Furthermore, we developed a method for measuring trace  $\text{Ag}^+$ ,  $\text{Cd}^{2+}$ , and  $\text{Cr}^{3+}$  ions in environmental water samples, which shows promise for future use. Our results indicate that NB-CDs can be used as fluorescent probes in biosystems because of their low toxicity and biocompatibility, making them ideal for cell imaging and detection of  $\text{Ag}^+$ ,  $\text{Cd}^{2+}$ , and  $\text{Cr}^{3+}$  ions.

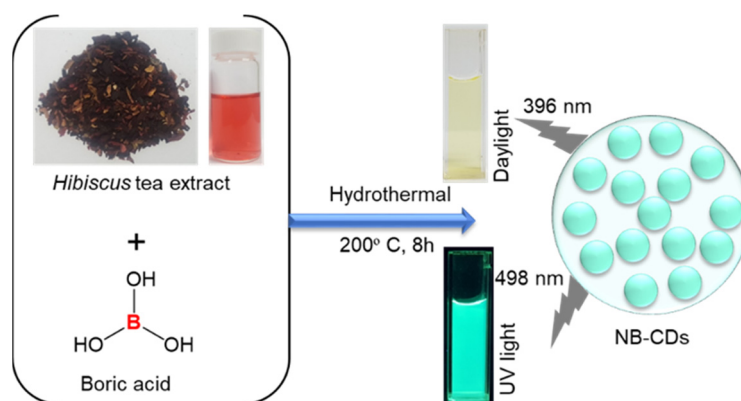


**Figure 1.** Schematic representation of the synthesized NB-CDs from Hibiscus herbal tea extract using boric acid as a doping agent.

## 2. Materials and Methods

### 2.1. Materials

*Hibiscus* herbal tea bags were purchased from a Coupang shopping market in South Korea (Coupang Product Number: 53362821–405057993). All chloride and nitrate salts and boric acid ( $\text{H}_3\text{BO}_3$ ) were obtained from Merck. The human colorectal carcinoma (HCT-116) cell line was obtained from the Korean Cell Line Bank (Seoul, Republic of Korea). The pH 1–13 solutions were adjusted using phosphoric acid (12.0 M) and sodium hydroxide (2.0 M) solution. pH measurements were carried out using a 720P pH meter (Istek instruments) with a combined standard round glass electrode. We used all other chemicals in this study to their analytical grade and used them exactly as received. The aqueous solutions were prepared with double-distilled water.

### 2.2. Synthesis of NB-CDs

First, *Hibiscus* herbal tea residue obtained after tea preparation was washed several times with water and dried at room temperature. Next, the dried tea residue was further ground into a fine powder and embrittled in liquid nitrogen. 2.0 g of this powder and 2.0 g of  $\text{H}_3\text{BO}_3$  were mixed in 40 mL of aqueous solution under magnetic stirring for 0.5 h. The mixture was then heated in an oven at 200 °C for 8 h in a Teflon-lined autoclave of 50 mL capacity. The mixture was then cooled to room temperature and centrifuged at 10,000 rpm to remove larger particles. Subsequently, the liquid was dialyzed for 48 h in a dialysis bag (1000 MWCO). After freeze drying for 24 h, CDs were obtained as a solid powder and stored in a refrigerator at 4 °C.

### 2.3. Characterizations

UV–Vis absorption spectra were measured using a UV 3220 (Optizen) spectrophotometer. A HITACHI F-2700 spectrofluorometer was used for the photoluminescence (PL) measurements. The fluorescence spectra of NB-CDs were measured using a standard quartz cuvette (3.0 mL). In both cases, the excitation and emission bandwidths were set to 5 nm at room temperature. FTIR analyses were conducted using an FT-IR spectrophotometer (Perkin Elmer) in the frequency range of 400–4000  $\text{cm}^{-1}$ . Powder X-ray diffraction (PXRD) patterns were recorded in the range of 10–80° on a PANalytical X'Pert Philips ( $\text{Cu-K}\alpha$  radiation) with a 1 min scan rate. X-ray photoelectron spectroscopy (XPS, Thermo Fisher Scientific, San Jose, CA USA) measurements were obtained using a Multilab-2000 spectrometer with Al  $\text{K}\alpha$  radiation monochromatized source. TEM with a 200 kV accelerating voltage (JEOL JEM-2100) was used to measure the size and shape of the NB-CDs.

### 2.4. Metal Ions Sensing

To prepare the photoluminescent probe, 20  $\mu\text{g}/\text{mL}$  of NB-CDs were dissolved in a HEPES buffer solution (pH = 7.4) under ambient conditions. Blank samples excited at

396 nm were measured for photoluminescence emission intensity at 498 nm. By adding different metal salts (chloride and nitrate), the selectivity toward metal ions, such as  $\text{Al}^{3+}$ ,  $\text{Ba}^{2+}$ ,  $\text{Ag}^+$ ,  $\text{Cd}^{2+}$ ,  $\text{Ca}^{2+}$ ,  $\text{Co}^{2+}$ ,  $\text{Cu}^{2+}$ ,  $\text{Fe}^{3+}$ ,  $\text{Cr}^{3+}$ ,  $\text{Ce}^{3+}$ ,  $\text{Zn}^{2+}$ ,  $\text{Mg}^{2+}$ ,  $\text{Mn}^{2+}$ ,  $\text{Ni}^{2+}$ ,  $\text{Na}^+$ ,  $\text{Pb}^{2+}$ ,  $\text{Sr}^{2+}$ ,  $\text{Sn}^{2+}$ , and  $\text{Ir}^{3+}$  (10  $\mu\text{M}$ ) was determined. The NB-CDs were tested for their sensitivity to  $\text{Ag}^+$ ,  $\text{Cd}^{2+}$  and  $\text{Cr}^{3+}$  ions at different concentrations. In the presence of  $\text{Ag}^+$ ,  $\text{Cd}^{2+}$  and  $\text{Cr}^{3+}$  ions, NB-CDs (20  $\mu\text{g}/\text{mL}$ ) were dissolved and mixed with solutions containing ions of concentration 0–10  $\mu\text{M}$ . After stirring for 30 s, the PL emission spectra were recorded at excitation and emission wavelengths of 396 nm and 410–700 nm, respectively.

### 2.5. Procedure for Cell Incubation and Imaging

MTT (3-(4,5-dimethylthiazol-2-yl)-2,5-diphenyltetrazolium bromide) assay was used to measure cell viability. HCT116 cells were seeded into 96-well plates at a density of  $4 \times 10^3$  cells/well. At 37 °C, an atmosphere of 5%  $\text{CO}_2$  and 95% air was applied to the cells after 12 h, followed by 0–100  $\mu\text{g}/\text{mL}$  (final concentration) of NB-CDs. Each well was incubated for 24 h at 37 °C and then treated with 10  $\mu\text{L}$  of diluted MTT. Incubation was continued for 4 h, followed by the addition of 100  $\mu\text{L}$  of DMSO. Finally, the cell survival rates were calculated. To prepare the cells for imaging, cells were washed three times with phosphate-buffered saline (PBS) and then incubated for 30 min with 20  $\mu\text{g}/\text{mL}$  of NB-CDs at 37 °C. HCT116 cells were incubated with 10  $\mu\text{M}$   $\text{Ag}^+$ ,  $\text{Cd}^{2+}$ , and  $\text{Cr}^{3+}$  ions for another 30 min at 37 °C and subsequently rinsed three times with PBS. Intracellular  $\text{Ag}^+$ ,  $\text{Cd}^{2+}$ , and  $\text{Cr}^{3+}$  ions were examined under a confocal microscope (Olympus, Tokyo, Japan, IX-81).

### 2.6. Determination of $\text{Ag}^+$ , $\text{Cd}^{2+}$ , and $\text{Cr}^{3+}$ Ions in Lake Water Samples

The lake water sample was collected from Gyeongsan High School premises near Yeungnam University, Republic of Korea, and used to prepare the required samples. The lake water was filtered through a 0.22  $\mu\text{m}$  membrane to remove the insoluble materials. The lake water sample (2.0 mL) was spiked with different  $\text{Ag}^+$ ,  $\text{Cd}^{2+}$ , and  $\text{Cr}^{3+}$  ions concentrations (1.0, 5.0 and 10  $\mu\text{M}$ ), respectively. Then, NB-CDs solution (20  $\mu\text{g}/\text{mL}$ ) was added, and experiments were run after equilibration for 1 min. All the different  $\text{Ag}^+$ ,  $\text{Cd}^{2+}$ , and  $\text{Cr}^{3+}$  ions concentrations with water samples were analyzed by using HITACHI F-2700 spectrofluorometer.

## 3. Results and Discussion

### 3.1. Optical Properties of NB-CDs

The optical properties of the NB-CDs were studied using UV-vis, and photoluminescence (PL) spectroscopy at room temperature. The UV-Visible and PL spectra depicted in Figure 2a show the absorption and excitation/emission intensities of the NB-CDs solution. The NB-CDs exhibited typical absorption and shoulder peaks at approximately 214 and 290 nm, respectively. In NB-CDs, this transition occurs in the C=C and C=N bonds of the  $\text{sp}^2$  carbon [33]. In addition, the excitation band at 396 nm is related to the  $n-\pi^*$  transition of the C=O defect on the surface of the NB-CDs [34]. The maximum excitation peak was observed at 396 nm, and the maximum emission peak was observed at 498 nm for the NB-CDs. When exposed to a 365 nm ultraviolet lamp, the dilution of the NB-CDs solution turned bright green. A change in the excitation wavelength from 320 to 500 nm affected the NB-CD water dispersion, as shown in Figure 2b (the strongest emission peak was around 498 nm), resulting from the relatively uniform surface state and size distribution. The excitation-dependent PL behavior of the NB-CDs was influenced by the particle size and surface state of the sample.

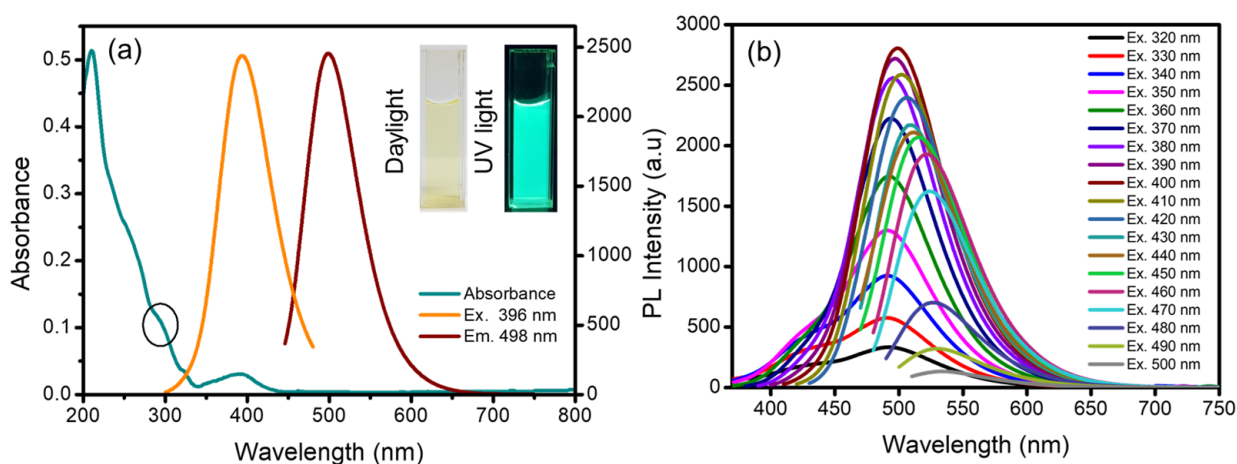


**Figure 2.** (a) UV–vis absorption spectra of the NB-CDs (5  $\mu\text{g}/\text{mL}$ ) and PL excitation and emission spectra of the NB-CDs (20  $\mu\text{g}/\text{mL}$ ). (Inset photographs of NB-CDs dispersions in water with daylight and UV illumination (365 nm), respectively). (b) PL spectra of the NB-CDs obtained at different excitation wavelengths.

### 3.2. Surface Analysis of NB-CDs

FTIR spectroscopy and PXRD analyses confirmed the presence of functional groups and crystallinity on the surface of the NB-CDs (Figure 3a,b). The absorption peaks at  $3332\text{ cm}^{-1}$  were attributed to the characteristic vibration bands of -OH bonds on the surface of the NB-CDs [35], as shown in Figure 3a. The sharp peak at the  $2986\text{ cm}^{-1}$  region in the NB-CD spectrum can be attributed to an asymmetric C-H stretching vibration. Furthermore, peaks were observed at  $2053$  and  $1649\text{ cm}^{-1}$ , indicating C-H, C-N stretching, and C-O bending vibrations, respectively. Furthermore, the NB-CDs exhibited distinct absorption bands at  $1316$ ,  $1087$ , and  $1033\text{ cm}^{-1}$ , which were associated with B-O stretching vibrations, C-B stretching modes, and B-O-H deformation vibrations. A powerful reducing element, boron reduces a wide range of compounds [36]. Thus, boron doping in the presence of boric acid may have reduced surface functional groups from -CO to -CH, which facilitates radiative recombination [37]. Due to their tunable properties, doping carbon nanomaterials with heteroatoms is highly appealing. Based on these findings, it is clear that the boric acid groups and NB-CD surface groups were successfully doped during particle formation. The high degree of graphitization in the NB-CDs was attributed to the disordered carbon atoms with a lattice spacing of 002 and 100 (Figure 3b). Moreover, the diffraction pattern of the NB-CDs shows peaks centered at approximately  $21.2^\circ$  and  $40.7^\circ$ , which are related to amorphous carbon [38].

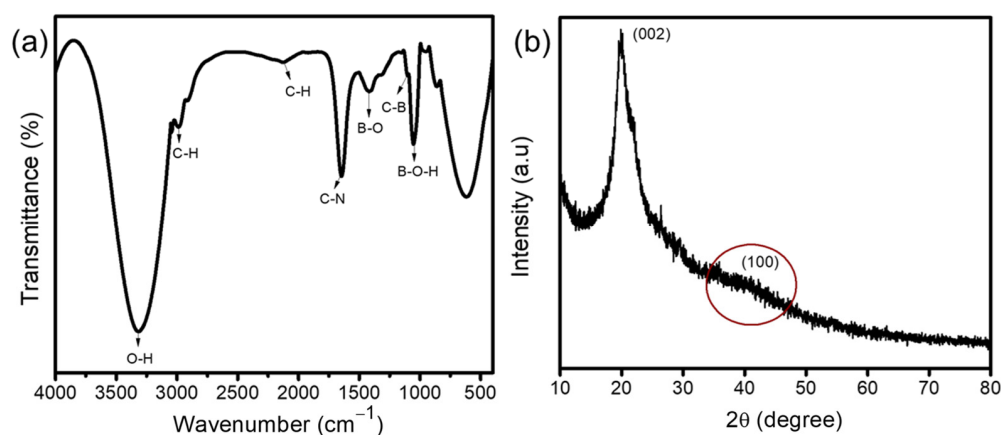


**Figure 3.** (a) FT-IR spectrum and (b) XRD pattern of NB-CDs.

XPS analysis was measured to the elemental species and their corresponding atom percentage in the obtained NB-CDs. As shown in Figure 4a, the full survey XPS spectrum of NB-CDs clearly exhibits four typical peaks at 401.2, 191.3, 284.6, and 531.4 eV, which are attributed to the characteristic binding energy signals of N1s, B1s, C1s, and O1s, and the atomic ratios were calculated to 18.28%, 12.47%, 60.99%, and 8.26%, respectively. The high-resolution N1s spectrum of the NB-CDs shows the presence of N–B, N–C, N–H, and N–O corresponding to the 397.8, 400.9, 402.3, and 403.1 eV [39], respectively, as shown in Figure 4b. The B1s spectrum is shown in Figure 4c and can be de-convoluted into three peaks that appear at 191.0, 191.8, and 192.7 eV and are attributed to the B–N B–C and B–O, respectively, which are well in agreement with the C1s, O1s, and FT-IR data. In Figure 4d, the C1s band was separated into four peaks at 284.1, 284.9, 286.3, and 288.9 eV, which are assigned to C–C/C=C, C–N, C–O, O–C=O [40], respectively. The O1s spectrum also shows three peaks at 532.1, 533.3, and 534.4 eV, assigned to O–B, C=O, and O=C–O, respectively (Figure 4e). These results demonstrate the NB-CDs are successfully functionalized by boric acid groups.

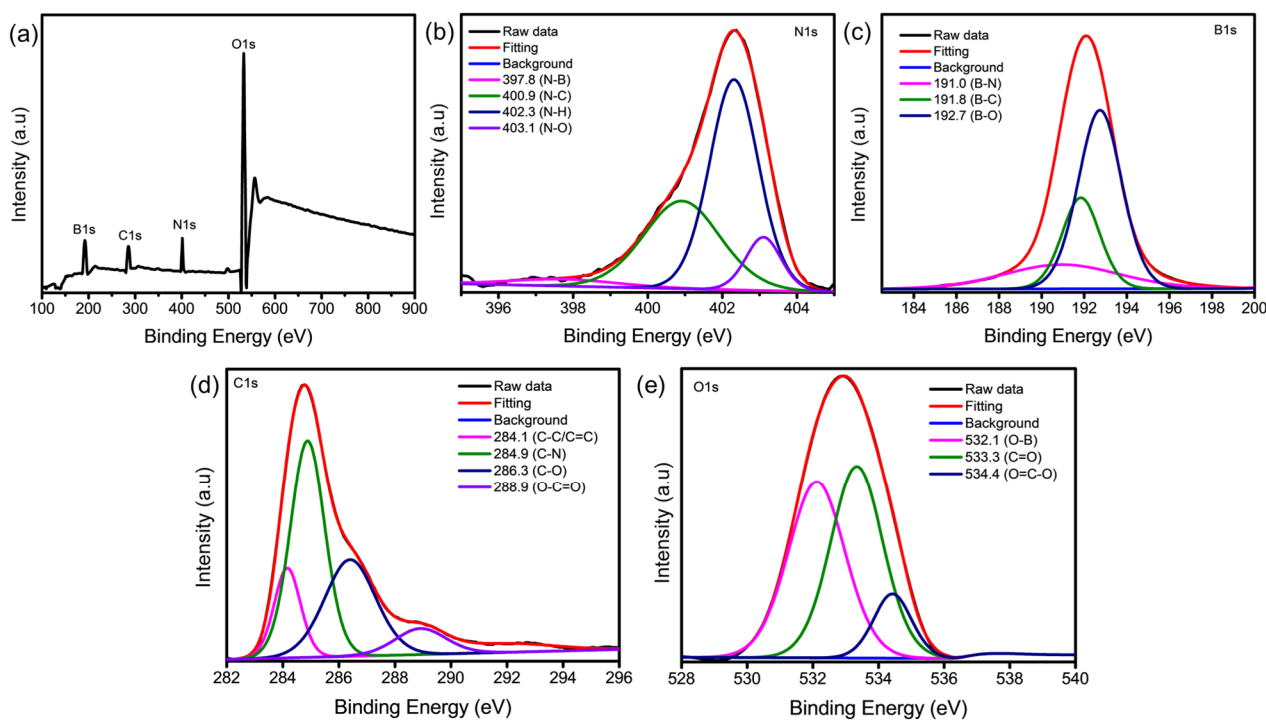


**Figure 4.** High-resolution XPS analysis of NB-CDs. (a) Survey spectrum, (b) N1s, (c) B1s, (d) C1s, and (e) O1s.

### 3.3. Morphology of NB-CDs

The NB-CDs appeared to be polydisperse spherical nanoparticles based on the TEM and high-resolution TEM images, as shown in Figure 5a. The size distribution histogram in inset Figure 5a shows that the as-prepared NB-CDs usually had a particle diameter between 2 and 8 nm and an average particle size of 6.2 nm [41]. The NB-CDs were imaged by HRTEM to reveal their crystallinity and lattice spacing of 0.23 nm (Figure 5b), with the same spacing as graphitic ( $sp^2$ ) carbon in the (100) plane [42]. The lattice constant of boron atoms is significantly smaller than that of pristine graphite (0.242 nm), suggesting that the doped boron atoms were introduced into the conjugated carbon backbone.

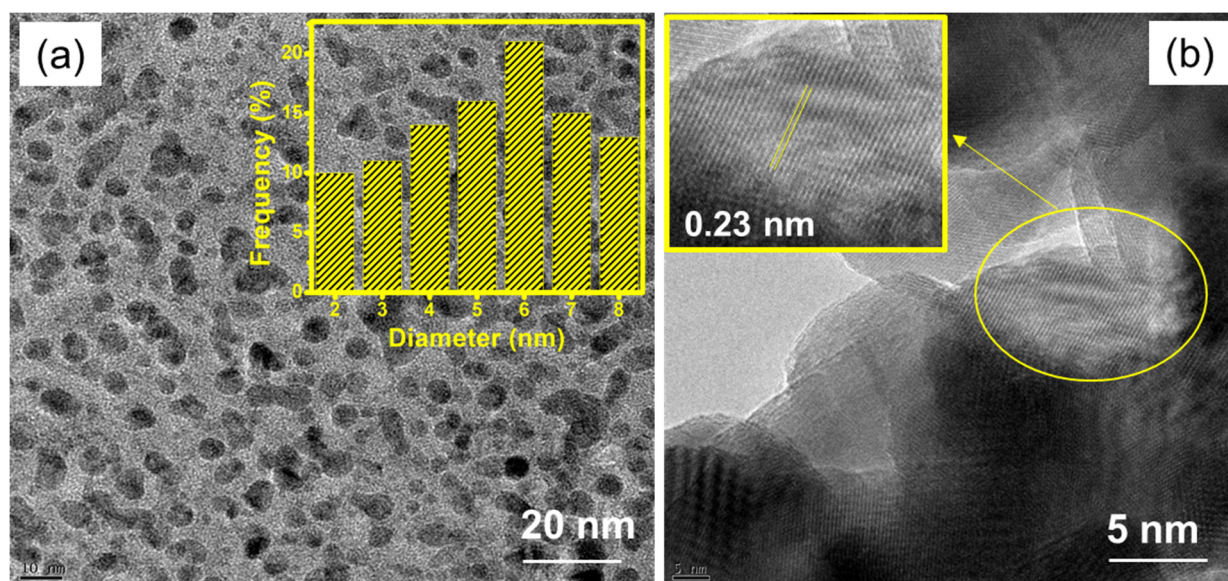


**Figure 5.** (a) TEM image (inset; size distribution histogram of NB-CDs) and (b) HRTEM images with lattice fringes of NB-CDs.

### 3.4. Chemosensors

To study the UV–Visible absorption and photoluminescent (PL) response of the NB-CDs (20  $\mu\text{g}/\text{mL}$ ) to various cations,  $\text{Al}^{3+}$ ,  $\text{Ba}^{2+}$ ,  $\text{Ag}^+$ ,  $\text{Cd}^{2+}$ ,  $\text{Ca}^{2+}$ ,  $\text{Co}^{2+}$ ,  $\text{Cu}^{2+}$ ,  $\text{Fe}^{3+}$ ,  $\text{Cr}^{3+}$ ,  $\text{Ce}^{3+}$ ,  $\text{Zn}^{2+}$ ,  $\text{Mg}^{2+}$ ,  $\text{Mn}^{2+}$ ,  $\text{Ni}^{2+}$ ,  $\text{Na}^+$ ,  $\text{Pb}^{2+}$ ,  $\text{Sr}^{2+}$ ,  $\text{Sn}^{2+}$ , and  $\text{Ir}^{3+}$  (10  $\mu\text{M}$ ) were added to a PBS buffer solution of NB-CDs (pH 7.4) as shown in Figure 6. Figure 6a shows the absorption spectra of the NB-CD sensor after adding  $\text{Ag}^+$ ,  $\text{Cd}^{2+}$ , and  $\text{Cr}^{3+}$  ions, which produce a significant blue shift with absorbance changes. The maximum emission intensity of the free NB-CDs was 498 nm when excited at 396 nm, as shown in Figure 6b. Marginal shifts at 481, 488, and 502 nm signaled the turn-on of PL emission from the NB-CDs sensor upon the addition of  $\text{Ag}^+$ ,  $\text{Cd}^{2+}$ , and  $\text{Cr}^{3+}$  ions (Figure 6b) [43–45]. Doped systems are enhanced by additional electrons being incorporated into the CDs, which result in enhanced electron transfer due to the hole-like structures formed in CDs by the doping of boron. By incorporating boron inside the CDs, the faster electron transfer process towards surface-attached NB-CDs should be perturbed. In contrast, after boron doping for CDs (NB-CDs), the reaction mixture led to further increasing PL intensity along with the  $\text{Ag}^+$ ,  $\text{Cd}^{2+}$ , and  $\text{Cr}^{3+}$  ions. Compared to other cations commonly found in physiological and environmental samples, NB-CDs more efficiently detect  $\text{Ag}^+$ ,  $\text{Cd}^{2+}$ , and  $\text{Cr}^{3+}$  ions. This observation suggests that the NB-CDs have good selectivity for detecting  $\text{Ag}^+$ ,  $\text{Cd}^{2+}$ , and  $\text{Cr}^{3+}$  ions. The addition of  $\text{Ag}^+$ ,  $\text{Cd}^{2+}$ , and  $\text{Cr}^{3+}$  ions immediately changed the color of the NB-CDs from yellow to colorless, and upon adding  $\text{Cr}^{3+}$  ions, the color changed from yellow to strongly yellow (Figure 6c). NB-CDs were exceptionally selective over other metal ions, as indicated by the color changes for each ion. Another characteristic of this probe is that it does not change color in the presence of other metal ions. Similarly,  $\text{Ag}^+$ ,  $\text{Cd}^{2+}$ , and  $\text{Cr}^{3+}$  ions showed excellent PL behavior under a UV lamp, changing from faint green to bluish-green and strong green PL (Figure 6c). The PL behavior of the other metal ions was not observed. The NB-CDs show color changes when cations are added because their surfaces coordinate with  $\text{Ag}^+$ ,  $\text{Cd}^{2+}$ , and  $\text{Cr}^{3+}$  ions. In the PL response test, all  $\text{Ag}^+$ ,  $\text{Cd}^{2+}$ , and  $\text{Cr}^{3+}$  ions displayed efficient “Off-On” fluorescence behaviors. The functional groups present on the surface of NB-CDs are responsible for binding with  $\text{Ag}^+$ ,  $\text{Cd}^{2+}$ , and  $\text{Cr}^{3+}$  ions. The presence of nitrogen (N) and oxygen (O) moieties on NB-CDs surfaces probably forms active binding sites towards  $\text{Ag}^+$ ,  $\text{Cd}^{2+}$ , and  $\text{Cr}^{3+}$  ions, thus making it an efficient PL enhancement sensor [46,47].

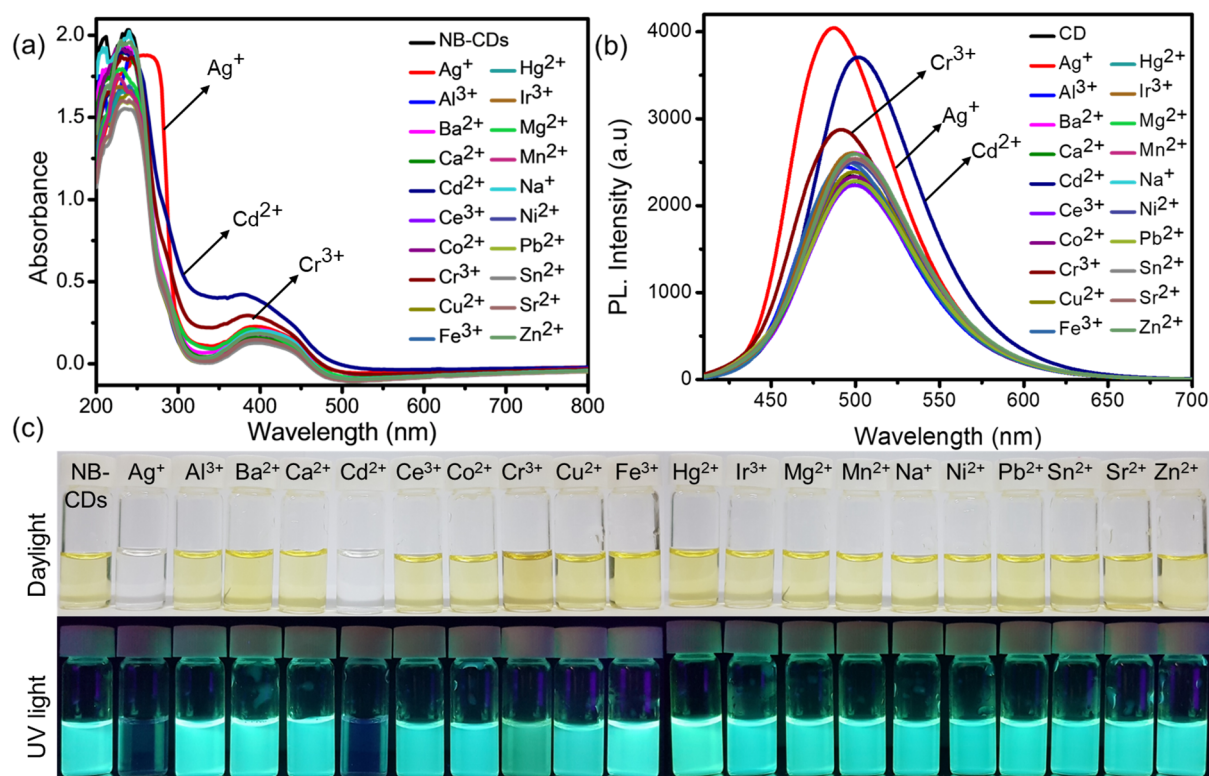


**Figure 6.** (a) UV–Visible absorption and (b) PL emission spectra of NB-CDs (20 µg/mL) solution in pH 7.4 PBS buffer solution before and after the addition of various metal ions (10 µM) and (c) the corresponding color changes of NB-CDs with absence and presence of metal ions under daylight and UV illumination (365 nm), respectively.

To evaluate the ion-sensing properties of the NB-CDs toward  $\text{Ag}^+$ ,  $\text{Cd}^{2+}$ , and  $\text{Cr}^{3+}$  ions, a PL titration experiment was conducted. Gradually increasing concentrations of  $\text{Ag}^+$ ,  $\text{Cd}^{2+}$ , and  $\text{Cr}^{3+}$  ions affected the PL characteristics. Figure 7a–c shows the changes in the PL spectra of NB-CDs upon the addition of  $\text{Ag}^+$ ,  $\text{Cd}^{2+}$ , and  $\text{Cr}^{3+}$  ions. While the sensor NB-CDs alone displayed negligible PL emission,  $\text{Ag}^+$ ,  $\text{Cd}^{2+}$ , and  $\text{Cr}^{3+}$  ions (10 µM) caused a prominent PL enhancement at wavelengths of 481, 488, and 502 nm, shifted from 498 nm, and the PL intensity of the peak showed a 46-, 18-, and 41-fold enhancement, respectively. Under a 365 nm UV lamp, photographs of the NB-CD solutions with and without  $\text{Ag}^+$ ,  $\text{Cd}^{2+}$ , and  $\text{Cr}^{3+}$  ions are shown in Figure 7a–c. The PL enhancement of NB-CDs by  $\text{Ag}^+$ ,  $\text{Cd}^{2+}$ , and  $\text{Cr}^{3+}$  ions is due to the obvious effect, which may be related to the strong binding between the N and O atoms on NB-CDs surfaces and the metal ions [46,47]. The NB-CDs emitted faint green PL in the presence of  $\text{Ag}^+$ ,  $\text{Cd}^{2+}$ , and  $\text{Cr}^{3+}$  ions PL enhancement with a significant shift to PL turn-on into a blueish green, and strong green was observed [48,49]. The reason for this phenomenon may be related to the strong binding of  $\text{Ag}^+$ ,  $\text{Cd}^{2+}$ , and  $\text{Cr}^{3+}$  ions to the N and O moieties functional groups of the NB-CDs. It is obvious that the relative photoluminescence intensity of NB-CDs shows a good linear relationship to the concentration of  $\text{Ag}^+$ ,  $\text{Cd}^{2+}$ , and  $\text{Cr}^{3+}$  ions in the range from 0–10 µM with a good correlation coefficient of 0.9922, 0.9974, and 0.9838 (Figure 7d–f). The fitted linear regression equation is  $I/I_0$  vs.  $\text{Ag}^+$ ,  $\text{Cd}^{2+}$ , and  $\text{Cr}^{3+}$  ions (µM), where  $I_0$  and  $I$  stand for the photoluminescence intensities of NB-CDs/ $\text{Ag}^+$ , NB-CDs/ $\text{Cd}^{2+}$ , and NB-CDs/ $\text{Cr}^{3+}$  systems in the absence and presence of  $\text{Ag}^+$ ,  $\text{Cd}^{2+}$ , and  $\text{Cr}^{3+}$  ions, respectively. Using Job’s method, the metal-ligand stoichiometry was determined by keeping the sum of the metal ions (10 µM) and NB-CDs (20 µg/mL) concentrations constant and varying the mole fraction of the metal ions from 0.1 to 0.9 mL [50]. When the molar ratio was 0.5, the maximum PL intensity was reproducibly observed, indicating that the NB-CDs bound  $\text{Ag}^+$ ,  $\text{Cd}^{2+}$ , and  $\text{Cr}^{3+}$  ions in a 1:1 (Figure 8a–c).

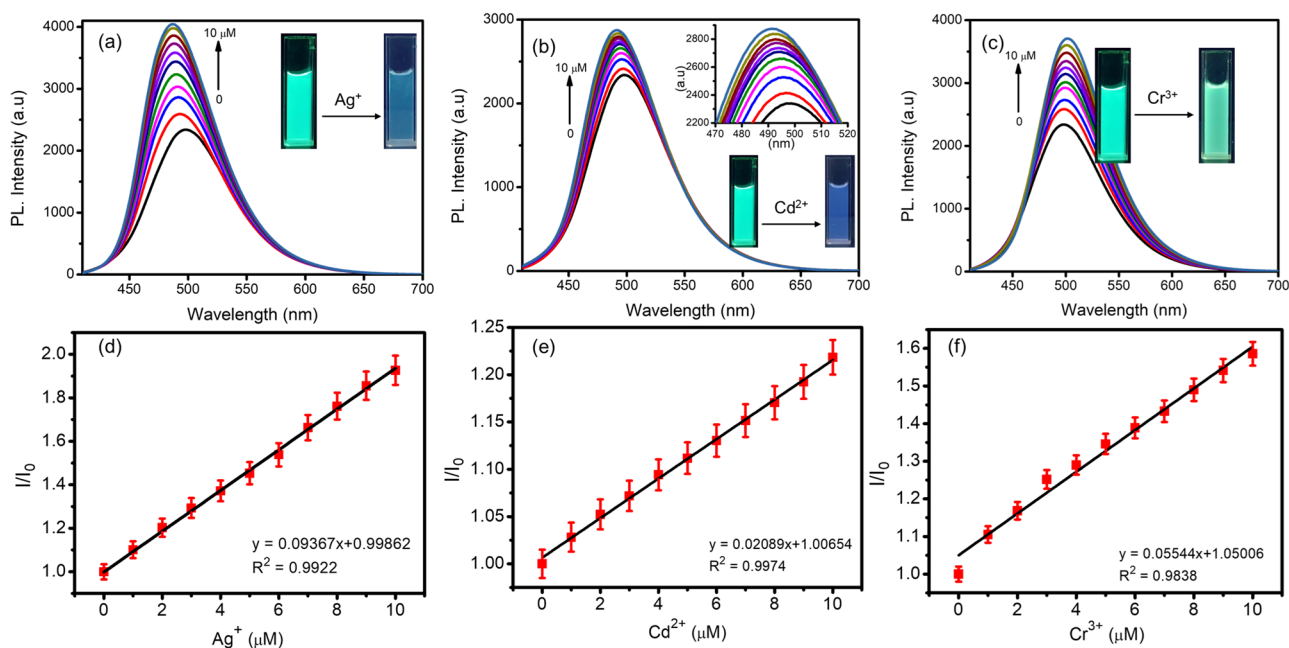


**Figure 7.** PL emission spectra of NB-CDs solution (20  $\mu\text{g}/\text{mL}$ ) in the presence of various concentrations (0–10  $\mu\text{M}$ ) of (a)  $\text{Ag}^+$ , (b)  $\text{Cd}^{2+}$ , and (c)  $\text{Cr}^{3+}$ . Inset photographs (a–c) show the PL color changes of NB-CDs with  $\text{Ag}^+$ ,  $\text{Cd}^{2+}$ , and  $\text{Cr}^{3+}$  ions. Inset Figure 7b, the enlarged PL emission intensity variation NB-CDs with various concentrations of  $\text{Cd}^{2+}$  ions. Linear relationship between the relative photoluminescence intensity of NB-CDs and concentration of (d)  $\text{Ag}^+$ , (e)  $\text{Cd}^{2+}$ , and (f)  $\text{Cr}^{3+}$  ions from 0–10  $\mu\text{M}$ .

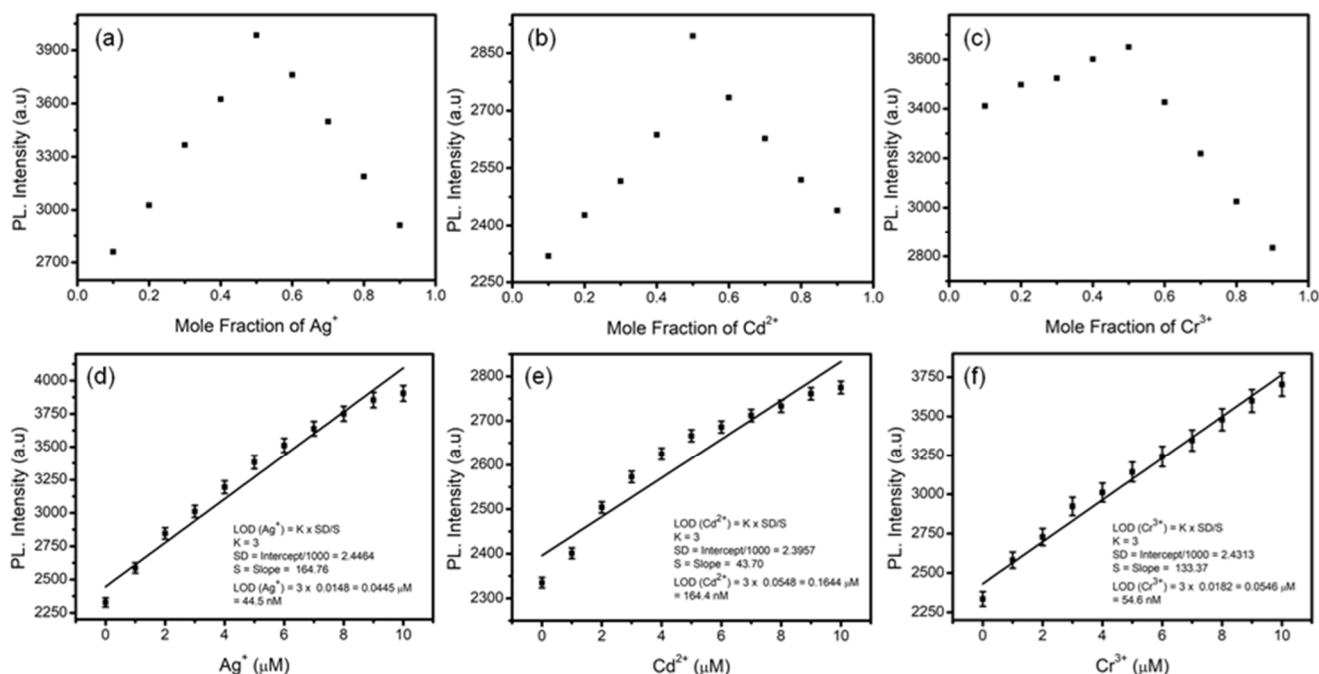


**Figure 8.** Job plot suggesting stoichiometry between chemosensor NB-CDs (20  $\mu\text{g}/\text{mL}$ ) and (a)  $\text{Ag}^+$ , (b)  $\text{Cd}^{2+}$ , and (c)  $\text{Cr}^{3+}$  ions (10  $\mu\text{M}$ ) = 1:1. The limit of detection calculations based on the PL intensity of NB-CDs with (d)  $\text{Ag}^+$ , (e)  $\text{Cd}^{2+}$ , and (f)  $\text{Cr}^{3+}$  ions (0–10  $\mu\text{M}$ ).

The detection limit (LOD) was determined from the following equation:  $K = 3\text{SD}/S$ , where SD is the standard deviation of the blank solution; S is the slope of the calibration curve [51]. The linear detection range and detection limit of the CDs for  $\text{Ag}^+$ ,  $\text{Cd}^{2+}$ , and  $\text{Cr}^{3+}$

ions reached 0–10  $\mu\text{M}$  and 44.5 nM, 164.4 nM, and 54.6 nM (Figure 8d–f). Furthermore, the obtained LOD is quite low in comparison with the WHO recommendations for  $\text{Ag}^+$ ,  $\text{Cd}^{2+}$ , and  $\text{Cr}^{3+}$  ions in drinking water. Thus, NB-CDs demonstrate the potential to measure  $\text{Ag}^+$ ,  $\text{Cd}^{2+}$ , and  $\text{Cr}^{3+}$  ions. The mechanisms of luminescence are closely related to CDs emission and include surface functional groups, surface oxidation, and molecular fluorescence. The exact mechanism behind CD fluorescence remains unclear because of CDs' substantial structural complexity. The photoluminescence changes of NB-CDs allow the quantification of  $\text{Ag}^+$ ,  $\text{Cd}^{2+}$ , and  $\text{Cr}^{3+}$  ion concentrations. In addition to  $\text{Ag}^+$ ,  $\text{Cd}^{2+}$ , and  $\text{Cr}^{3+}$  ions, the synthesized NB-CDs sensor was insignificant for all the other tested metal ions. The selectivity and interference selectivity of the NB-CDs, NB-CDs/ $\text{Ag}^+$ , NB-CDs/ $\text{Cd}^{2+}$ , and NB-CDs/ $\text{Cr}^{3+}$  systems toward various metal ions are plotted as a bar graph in Figure 9. Based on this sensing system,  $\text{Ag}^+$ ,  $\text{Cd}^{2+}$ , and  $\text{Cr}^{3+}$  ions have good selectivity compared to the other metal ions.

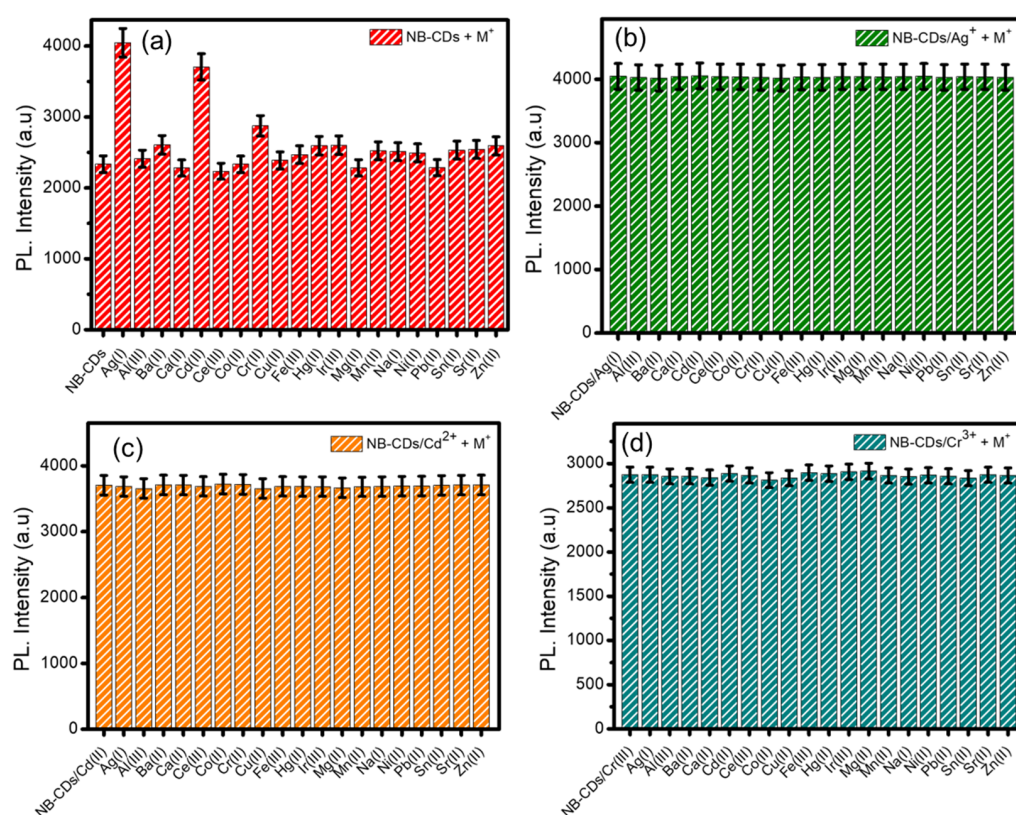


**Figure 9.** Histogram of the PL selectivity and interferences of (a) NB-CDs, (b) NB-CDs/ $\text{Ag}^+$ , (c) NB-CDs/ $\text{Cd}^{2+}$ , and (d) NB-CDs/ $\text{Cr}^{3+}$  systems in the presence of other metal ions.

### 3.5. Living Cell Imaging

HCT-116 cells were tested for cytotoxicity and cellular imaging using the MTT assay to further demonstrate the applicability of NB-CDs in biological samples. HCT-116 cells were incubated for 24 h with the chemosensor NB-CDs at various concentrations (0, 20, 40, 60, 80, and 100  $\mu\text{g}/\text{mL}$ ) as shown in Figure 10a. Under our experimental conditions, more than 97% of the HCT-116 cells were viable, indicating that NB-CDs were not cytotoxic [52]. Thus, the NB-CDs can detect and image intracellular activities. Incubating HCT-116 cells at 37  $^{\circ}\text{C}$  for 0.5 h with NB-CDs (20  $\mu\text{g}/\text{mL}$ ) followed by 0.5 h with chloride salts of  $\text{Ag}^+$ ,  $\text{Cd}^{2+}$ , and  $\text{Cr}^{3+}$  ions (10  $\mu\text{M}$ ) was conducted. The cells were then washed three times with PBS. Phase contrast, fluorescence, and overlay images were captured before and after the addition of  $\text{Ag}^+$ ,  $\text{Cd}^{2+}$ , and  $\text{Cr}^{3+}$ , as shown in Figure 10b. Faint green fluorescence was observed when HCT-116 cells were incubated with NB-CDs. After incubation with  $\text{Ag}^+$ ,  $\text{Cd}^{2+}$ , and  $\text{Cr}^{3+}$ , living cells showed blue and strong green fluorescence [53]. NB-CDs exhibited excellent cell

membrane permeability in an overlay of fluorescence and phase-contrast images, indicating effective fluorescence signals [54]. Based on these findings, the NB-CDs can be used to detect  $\text{Ag}^+$ ,  $\text{Cd}^{2+}$ , and  $\text{Cr}^{3+}$  in living cells.

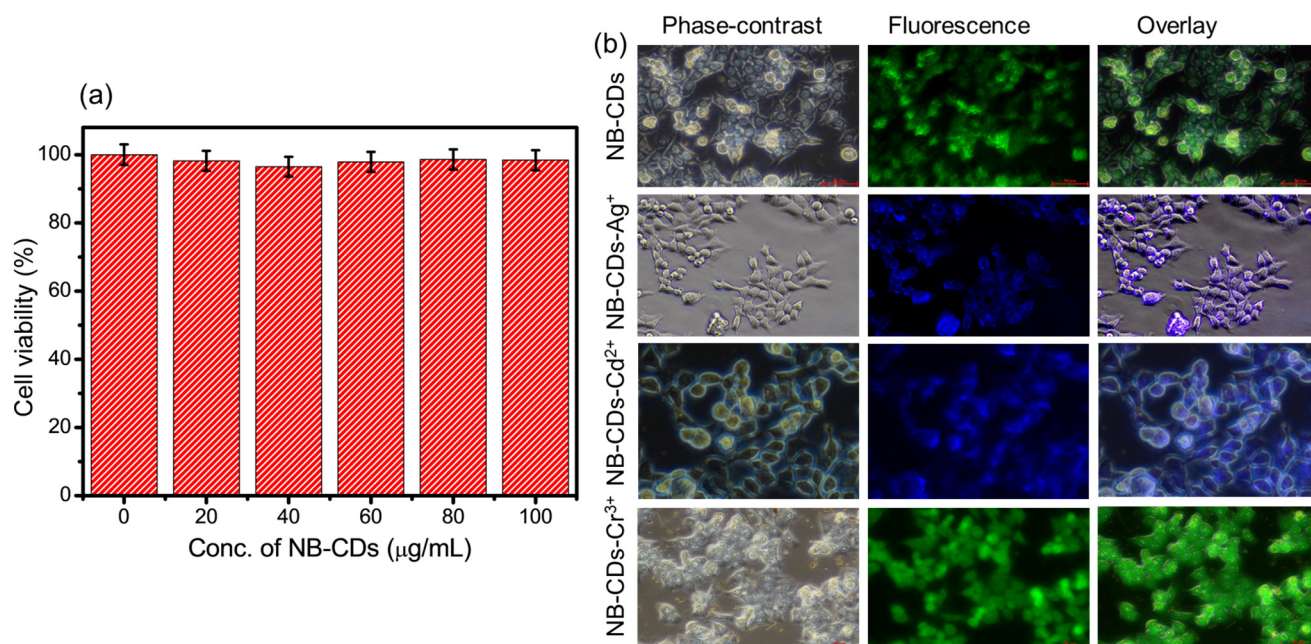


**Figure 10.** (a) Cell viability (HCT-116) measurement using the MTT assay with various concentrations of NB-CDs (b) Phase-contrast, fluorescence, and overlay images of NB-CDs, NB-CDs/ $\text{Ag}^+$ , NB-CDs/ $\text{Cd}^{2+}$ , and NB-CDs/ $\text{Cr}^{3+}$  complexes.

### 3.6. Real Sample Analysis

In lake water samples, NB-CDs sensors were validated for the selective detection of  $\text{Ag}^+$ ,  $\text{Cd}^{2+}$ , and  $\text{Cr}^{3+}$  ions. For analysis, the lake water samples were spiked with various concentrations of  $\text{Ag}^+$ ,  $\text{Cd}^{2+}$ , and  $\text{Cr}^{3+}$  ions and then analyzed by the proposed method. The results obtained from each sample were repeated thrice and are summarized in Table 1. Based on the analytical results, the recoveries ranged from 97.2% to 104.2%, whereas the relative errors (0.98–2.78%) were less than 3%. Consequently, this method can be used to reliably detect  $\text{Ag}^+$ ,  $\text{Cd}^{2+}$ , and  $\text{Cr}^{3+}$  ions in practical samples.

**Table 1.** Analytical results for determining  $\text{Ag}^+$ ,  $\text{Cd}^{2+}$ , and  $\text{Cr}^{3+}$  ions in a lake water sample.

Metal Ions	Spiked Amount (µM)	Recovered Amount (µM)	% Recovery ± SD (n = 3)
$\text{Ag}^+$	1	1.03	103.4 ± 1.28
	5	4.86	97.2 ± 2.14
	10	9.87	98.7 ± 1.97
$\text{Cd}^{2+}$	1	1.04	104.2 ± 2.78
	5	5.09	101.8 ± 1.49
	10	10.12	101.2 ± 2.11
$\text{Cr}^{3+}$	1	0.99	99.0 ± 0.98
	5	4.99	99.8 ± 1.73
	10	10.08	100.8 ± 2.64

## 4. Conclusions

In this study, we developed photoluminescent NB-CDs from *Hibiscus* herbal tea extract co-doped with boric acid via a hydrothermal method for the highly selective and sensitive detection of heavy metal ions. The NB-CDs were comprehensively characterized using UV–

vis, PL, FTIR, XRD, XPS, and TEM analysis. The NB-CDs exhibited good water solubility, high photoluminescence, and good photostability. The NB-CDs exhibited a strong emission peak at 498 nm when excited at 396 nm, with a quantum yield (9.2%). The NB-CDs are spherical with average diameters of  $6.2 \pm 0.5$  nm in the range of 2.0–8.0 nm. In addition, the NB-CDs showed excellent selectivity and sensitivity and were used as a photoluminescent probe to detect  $\text{Ag}^+$ ,  $\text{Cd}^{2+}$ , and  $\text{Cr}^{3+}$  ions in aqueous solutions with the detection limit of 44.5, 164.4, and 54.6 nM, respectively, with a wide concentration range of 0–10  $\mu\text{M}$ . Moreover, multicolor photoluminescent CDs have been successfully applied in cell imaging at nontoxic concentrations, suggesting that they are a promising resource for biological imaging. The sensor was successfully used to measure trace amounts of  $\text{Ag}^+$ ,  $\text{Cd}^{2+}$ , and  $\text{Cr}^{3+}$  ions in real water samples. This study provides new insights for the development of low-cost, selective, and environmentally friendly sensors for the detection of  $\text{Ag}^+$ ,  $\text{Cd}^{2+}$ , and  $\text{Cr}^{3+}$  ions.

**Author Contributions:** Conceptualization, methodology, writing—original draft preparation, S.M. methodology, investigation, N.A.; validation and review editing, K.S.V.; methodology, investigation, M.R.K.; methodology, investigation, S.P.; methodology, investigation, S.Y.; validation and review editing, Y.R.L. All authors have read and agreed to the published version of the manuscript.

**Funding:** This work was supported by an NRF grant funded by the Korean government (2021R1F1A1061566). This research was supported by Korea Basic Science Institute (National Research Facilities and Equipment Center) grant funded by the Ministry of Education (2019R1A6C1010046). The authors would also like to thank the Researchers Supporting Project Number (RSPD-2023R668), King Saud University, Riyadh, Saudi Arabia.

**Institutional Review Board Statement:** Not applicable.

**Informed Consent Statement:** Not applicable.

**Data Availability Statement:** The data presented in this study are available upon request from the corresponding author.

**Conflicts of Interest:** The authors declare no conflict of interest.

## References

1. Mitra, S.; Chakraborty, A.J.; Tareq, A.M.; Emran, T.B.; Nainu, F.; Khusro, A.; Idris, A.M.; Khandaker, M.U.; Osman, H.; Alhumaydhi, F.A.; et al. Impact of Heavy Metals on the Environment and Human Health: Novel Therapeutic Insights to Counter the Toxicity. *J. King Saud Univ. Sci.* **2022**, *34*, 101865. [[CrossRef](#)]
2. Herschy, R.W. Water Quality for Drinking: WHO Guidelines. In *Encyclopedia of Lakes and Reservoirs*; Springer: Berlin/Heidelberg, Germany, 2012; pp. 876–883. [[CrossRef](#)]
3. United States Environmental Protection Agency. *Us-Epa Guidance for Assessing Chemical Contaminant Data for Use in Fish Advisories, Volume 2: Risk Assessment and Fish Consumption Limits*, 3rd ed.; United States Environmental Protection Agency: Washington, DC, USA, 2000; Volume 1, pp. 1–383.
4. Liu, W.; Liu, Y.; Yuan, Z.; Lu, C. Recent Advances in the Detection and Removal of Heavy Metal Ions Using Functionalized Layered Double Hydroxides: A Review. *Ind. Chem. Mater.* **2023**, *1*, 79–92. [[CrossRef](#)]
5. Chen, L.; Tian, X.; Xia, D.; Nie, Y.; Lu, L.; Yang, C.; Zhou, Z. Novel Colorimetric Method for Simultaneous Detection and Identification of Multimetal Ions in Water: Sensitivity, Selectivity, and Recognition Mechanism. *ACS Omega* **2019**, *4*, 5915–5922. [[CrossRef](#)]
6. Lian, J.; Xu, Q.; Wang, Y.; Meng, F. Recent Developments in Fluorescent Materials for Heavy Metal Ions Analysis from the Perspective of Forensic Chemistry. *Front. Chem.* **2020**, *8*, 593291. [[CrossRef](#)] [[PubMed](#)]
7. Choi, S.H.; Kim, J.Y.; Choi, E.M.; Lee, M.Y.; Yang, J.Y.; Ho Lee, G.; Kim, K.S.; Yang, J.S.; Russo, R.E.; Yoo, J.H.; et al. Heavy Metal Determination by Inductively Coupled Plasma–Mass Spectrometry (ICP-MS) and Direct Mercury Analysis (DMA) and Arsenic Mapping by Femtosecond (Fs)–Laser Ablation (LA) ICP-MS in Cereals. *Anal. Lett.* **2019**, *52*, 496–510. [[CrossRef](#)]
8. Heo, E.-Y.; Ko, Y.-I.; Bae, J.-S. Detection of Heavy Metal Ions in Aqueous Solution Using Direct Dye Chemosensors. *Text. Color. Finish.* **2009**, *21*, 51–57. [[CrossRef](#)]
9. Li, L.; Wang, J.; Xu, S.; Li, C.; Dong, B. Recent Progress in Fluorescent Probes For Metal Ion Detection. *Front. Chem.* **2022**, *10*, 875241. [[CrossRef](#)]
10. Torres Landa, S.D.; Reddy Bogireddy, N.K.; Kaur, I.; Batra, V.; Agarwal, V. Heavy Metal Ion Detection Using Green Precursor Derived Carbon Dots. *iScience* **2022**, *25*, 103816. [[CrossRef](#)]

11. Soumya, K.; More, N.; Choppadandi, M.; Aishwarya, D.A.; Singh, G.; Kapusetti, G. Biomedical Technology A Comprehensive Review on Carbon Quantum Dots as an Effective Photosensitizer and Drug Delivery System for Cancer Treatment. *Biomed. Technol.* **2023**, *4*, 11–20. [[CrossRef](#)]
12. Gao, S.; Yan, S.; Zhao, H.; Nathan, A. Emerging Applications. *Touch-Based Hum. Mach. Interact.* **2021**, 179–229. [[CrossRef](#)]
13. Liu, J.; Li, R.; Yang, B. Carbon Dots: A New Type of Carbon-Based Nanomaterial with Wide Applications. *ACS Cent. Sci.* **2020**, *6*, 2179–2195. [[CrossRef](#)] [[PubMed](#)]
14. Ghosal, K.; Ghosh, A. Carbon Dots: The next Generation Platform for Biomedical Applications. *Mater. Sci. Eng. C* **2019**, *96*, 887–903. [[CrossRef](#)] [[PubMed](#)]
15. Jiang, X.; Qin, D.; Mo, G.; Feng, J.; Yu, C.; Mo, W.; Deng, B. Ginkgo Leaf-Based Synthesis of Nitrogen-Doped Carbon Quantum Dots for Highly Sensitive Detection of Salazosulapyridine in Mouse Plasma. *J. Pharm. Biomed. Anal.* **2019**, *164*, 514–519. [[CrossRef](#)] [[PubMed](#)]
16. Gupta, D.A.; Desai, M.L.; Malek, N.I.; Kailasa, S.K. Fluorescence Detection of Fe<sup>3+</sup> Ion Using Ultra-Small Fluorescent Carbon Dots Derived from Pineapple (Ananas Comosus): Development of Miniaturized Analytical Method. *J. Mol. Struct.* **2020**, *1216*, 128343. [[CrossRef](#)]
17. Chen, K.; Qing, W.; Hu, W.; Lu, M.; Wang, Y.; Liu, X. On-off-on Fluorescent Carbon Dots from Waste Tea: Their Properties, Antioxidant and Selective Detection of CrO<sub>4</sub><sup>2-</sup>, Fe<sup>3+</sup>, Ascorbic Acid and L-Cysteine in Real Samples. *Spectrochim. Acta Part A Mol. Biomol. Spectrosc.* **2019**, *213*, 228–234. [[CrossRef](#)]
18. Shivaji, K.; Mani, S.; Ponnurugan, P.; De Castro, C.S.; Lloyd Davies, M.; Balasubramanian, M.G.; Pitchaimuthu, S. Green-Synthesis-Derived CdS Quantum Dots Using Tea Leaf Extract: Antimicrobial, Bioimaging, and Therapeutic Applications in Lung Cancer Cells. *ACS Appl. Nano Mater.* **2018**, *1*, 1683–1693. [[CrossRef](#)]
19. Jiao, X.Y.; Li, L.S.; Qin, S.; Zhang, Y.; Huang, K.; Xu, L. The Synthesis of Fluorescent Carbon Dots from Mango Peel and Their Multiple Applications. *Colloids Surf. A Physicochem. Eng. Asp.* **2019**, *577*, 306–314. [[CrossRef](#)]
20. Nguyen, T.N.; Le, P.A.; Phung, V.B.T. Facile Green Synthesis of Carbon Quantum Dots and Biomass-Derived Activated Carbon from Banana Peels: Synthesis and Investigation. *Biomass Convers. Biorefinery* **2022**, *12*, 2407–2416. [[CrossRef](#)]
21. Quan, C.; Zhou, Y.; Wang, J.; Wu, C.; Gao, N. Biomass-Based Carbon Materials for CO<sub>2</sub> capture: A Review. *J. CO<sub>2</sub> Util.* **2023**, *68*, 102373. [[CrossRef](#)]
22. McKay, D.L.; Chen, C.Y.O.; Saltzman, E.; Blumberg, J.B. *Hibiscus sabdariffa* L. Tea (Tisane) Lowers Blood Pressure in Prehypertensive and Mildly Hypertensive Adults. *J. Nutr.* **2010**, *140*, 298–303. [[CrossRef](#)]
23. Malacrida, A.; Erriquez, J.; Hashemi, M.; Rodriguez-Menendez, V.; Cassetti, A.; Cavaletti, G.; Miloso, M. Evaluation of Antitumoral Effect of Hibiscus Sabdariffa Extract on Human Breast Cancer Cells. *Biochem. Biophys. Rep.* **2022**, *32*, 101353. [[CrossRef](#)] [[PubMed](#)]
24. Zulfiqar, S.; Marshall, L.J.; Boesch, C. Hibiscus Sabdariffa Inhibits  $\alpha$ -Glucosidase Activity in Vitro and Lowers Postprandial Blood Glucose Response in Humans. *Hum. Nutr. Metab.* **2022**, *30*, 200164. [[CrossRef](#)]
25. Frész, T.; Nagy, E.; Hilbert, Á.; Tomcsányi, J. The Role of Flavonoids in False Positive Digoxin Assays Caused by the Consumption of Hibiscus Flower and Rose Hip Tea. *Int. J. Cardiol.* **2014**, *171*, 273–274. [[CrossRef](#)] [[PubMed](#)]
26. Gallaher, R.N.; Gallaher, K.; Marshall, A.J.; Marshall, A.C. Mineral Analysis of Ten Types of Commercially Available Tea. *J. Food Compos. Anal.* **2006**, *19*, 53–57. [[CrossRef](#)]
27. Judith, J.V.; Vasudevan, N. Synthesis of Nanomaterial from Industrial Waste and Its Application in Environmental Pollutant Remediation. *Environ. Eng. Res.* **2022**, *27*, 200672. [[CrossRef](#)]
28. Abd Elkodous, M.; Hamad, H.A.; Abdel Maksoud, M.I.A.; Ali, G.A.M.; El Abboubi, M.; Bedir, A.G.; Eldeeb, A.A.; Ayed, A.A.; Gargar, Z.; Zaki, F.S.; et al. Cutting-Edge Development in Waste-Recycled Nanomaterials for Energy Storage and Conversion Applications. *Nanotechnol. Rev.* **2022**, *11*, 2215–2294. [[CrossRef](#)]
29. Barman, M.K.; Patra, A. Current Status and Prospects on Chemical Structure Driven Photoluminescence Behaviour of Carbon Dots. *J. Photochem. Photobiol. C Photochem. Rev.* **2018**, *37*, 1–22. [[CrossRef](#)]
30. Deng, Y.; Long, Y.; Song, A.; Wang, H.; Xiang, S.; Qiu, Y.; Ge, X.; Golberg, D.; Weng, Q. Boron Dopants in Red-Emitting B and N Co-Doped Carbon Quantum Dots Enable Targeted Imaging of Lysosomes. *ACS Appl. Mater. Interfaces* **2023**, *15*, 17045–17053. [[CrossRef](#)]
31. Nabid, M.R.; Bide, Y.; Fereidouni, N. Boron and Nitrogen Co-Doped Carbon Dots as a Metal-Free Catalyst for Hydrogen Generation from Sodium Borohydride. *New J. Chem.* **2016**, *40*, 8823–8828. [[CrossRef](#)]
32. Cheng, S.; Zhang, J.; Liu, Y.; Wang, Y.; Xiao, Y.; Zhang, Y. High Quantum Yield Nitrogen and Boron Co-Doped Carbon Dots for Sensing Ag<sup>+</sup>, Biological Imaging and Fluorescent Inks. *Anal. Methods* **2021**, *13*, 5523–5531. [[CrossRef](#)]
33. Luo, B.; Yang, H.; Zhou, B.; Ahmed, S.M.; Zhang, Y.; Liu, H.; Liu, X.; He, Y.; Xia, S. Facile Synthesis of Luffa Sponge Activated Carbon Fiber Based Carbon Quantum Dots with Green Fluorescence and Their Application in Cr(VI) Determination. *ACS Omega* **2020**, *5*, 5540–5547. [[CrossRef](#)] [[PubMed](#)]
34. Ustun, O.; Karadag, S.N.; Mazlumoglu, H.; Yilmaz, A. PH-Sensitive Fluorescence Emission of Boron/Nitrogen. *Coatings* **2023**, *13*, 456. [[CrossRef](#)]
35. Wang, S.; Sun, W.; Yang, D.S.; Yang, F. Soybean-Derived Blue Photoluminescent Carbon Dots. *Beilstein J. Nanotechnol.* **2020**, *11*, 606–619. [[CrossRef](#)]
36. Bissinger, P.; Braunschweig, H.; Damme, A.; Hörl, C.; Krummenacher, I.; Kupfer, T. Boron as a Powerful Reductant: Synthesis of a Stable Boron-Centered Radical-Anion Radical-Cation Pair. *Angew. Chem. Int. Ed.* **2015**, *54*, 359–362. [[CrossRef](#)]

37. Zhu, S.; Zhang, J.; Tang, S.; Qiao, C.; Wang, L.; Wang, H.; Liu, X.; Li, B.; Li, Y.; Yu, W.; et al. Surface Chemistry Routes to Modulate the Photoluminescence of Graphene Quantum Dots: From Fluorescence Mechanism to up-Conversion Bioimaging Applications. *Adv. Funct. Mater.* **2012**, *22*, 4732–4740. [[CrossRef](#)]
38. Hossain, M.D.; Zhang, Q.; Cheng, T.; Goddard, W.A.; Luo, Z. Graphitization of Low-Density Amorphous Carbon for Electrocatalysis Electrodes from ReaxFF Reactive Dynamics. *Carbon* **2021**, *183*, 940–947. [[CrossRef](#)]
39. Mohandoss, S.; Palanisamy, S.; You, S.; Shim, J.J.; Lee, Y.R. Rapid Detection of Silver Ions Based on Luminescent Carbon Nanodots for Multicolor Patterning, Smartphone Sensors, and Bioimaging Applications. *Anal. Methods* **2021**, *13*, 5719–5726. [[CrossRef](#)]
40. Mohandoss, S.; Palanisamy, S.; Priya, V.V.; Mohan, S.K.; Shim, J.-J.; Yelithao, K.; You, S.; Lee, Y.R. Excitation-Dependent Multiple Luminescence Emission of Nitrogen and Sulfur Co-Doped Carbon Dots for Cysteine Sensing, Bioimaging, and Photoluminescent Ink Applications. *Microchem. J.* **2021**, *167*, 106280. [[CrossRef](#)]
41. Issa, M.A.; Abidin, Z.Z. Sustainable Development of Enhanced Luminescence Polymer-Carbon Dots Composite Film for Rapid Cd<sup>2+</sup> Removal from Wastewater. *Molecules* **2020**, *25*, 3541. [[CrossRef](#)]
42. Lei, M.; Xie, Y.; Chen, L.; Liu, X.; Yang, Y.; Zheng, J.; Li, Q. Surface State Modulation of Blue-Emitting Carbon Dots with High Quantum Yield and High Product Yield. *RSC Adv.* **2022**, *12*, 27431–27441. [[CrossRef](#)]
43. Zhao, L.; Li, J.; Sui, D.; Wang, Y. Highly Selective Fluorescence Chemosensors Based on Functionalized SBA-15 for Detection of Ag<sup>+</sup> in Aqueous Media. *Sens. Actuators B Chem.* **2017**, *242*, 1043–1049. [[CrossRef](#)]
44. Wang, Y.; Hu, X.; Wang, L.; Shang, Z.; Chao, J.; Jin, W. A New Acridine Derivative as a Highly Selective “off-on” Fluorescence Chemosensor for Cd<sup>2+</sup> in Aqueous Media. *Sens. Actuators B Chem.* **2011**, *156*, 126–131. [[CrossRef](#)]
45. Gupta, V.K.; Mergu, N.; Singh, A.K. Rhodamine-Derived Highly Sensitive and Selective Colorimetric and off-on Optical Chemosensors for Cr<sup>3+</sup>. *Sens. Actuators B Chem.* **2015**, *220*, 420–432. [[CrossRef](#)]
46. Wang, S.; Deng, G.; Yang, J.; Chen, H.; Long, W.; She, Y.; Fu, H. Carbon Dot- and Gold Nanocluster-Based Three-Channel Fluorescence Array Sensor: Visual Detection of Multiple Metal Ions in Complex Samples. *Sens. Actuators B Chem.* **2022**, *369*, 132194. [[CrossRef](#)]
47. Sadhanala, H.K.; Pagidi, S.; Gedanken, A. High Quantum Yield Boron-Doped Carbon Dots: A Ratiometric Fluorescent Probe for Highly Selective and Sensitive Detection of Mg<sup>2+</sup> ions. *J. Mater. Chem. C* **2021**, *9*, 1632–1640. [[CrossRef](#)]
48. Preeyanka, N.; Sarkar, M. Probing How Various Metal Ions Interact with the Surface of QDs: Implication of the Interaction Event on the Photophysics of QDs. *Langmuir* **2021**, *37*, 6995–7007. [[CrossRef](#)]
49. Fernandes, R.S.; Shetty, N.S.; Mahesha, P.; Gaonkar, S.L. *A Comprehensive Review on Thiophene Based Chemosensors*; Springer US: Berlin/Heidelberg, Germany, 2022; Volume 32, ISBN 0123456789.
50. Mabrouk, M.; Hammad, S.F.; Abdelaziz, M.A.; Mansour, F.R. Ligand Exchange Method for Determination of Mole Ratios of Relatively Weak Metal Complexes: A Comparative Study. *Chem. Cent. J.* **2018**, *12*, 143. [[CrossRef](#)]
51. Saadati, N.; Abdullah, M.P.; Zakaria, Z.; Sany, S.B.T.; Rezayi, M.; Hassonizadeh, H. Limit of Detection and Limit of Quantification Development Procedures for Organochlorine Pesticides Analysis in Water and Sediment Matrices. *Chem. Cent. J.* **2013**, *7*, 1. [[CrossRef](#)]
52. Romano, M.R.; Ferrara, M.; Gatto, C.; Ferrari, B.; Giurgola, L.; Tóthová, J.D. Evaluation of Cytotoxicity of Perfluorocarbons for Intraocular Use by Cytotoxicity Test in Vitro in Cell Lines and Human Donor Retina Ex Vivo. *Transl. Vis. Sci. Technol.* **2019**, *8*, 24. [[CrossRef](#)]
53. La Rocca, A.; De Gregorio, V.; Lagreca, E.; Vecchione, R.; Netti, P.A.; Imparato, G. Colorectal Cancer Bioengineered Microtissues as a Model to Replicate Tumor-ECM Crosstalk and Assess Drug Delivery Systems In Vitro. *Int. J. Mol. Sci.* **2023**, *24*, 5678. [[CrossRef](#)]
54. Thirumalaivasan, N.; Wu, S.P. Bright Luminescent Carbon Dots for Multifunctional Selective Sensing and Imaging Applications in Living Cells. *ACS Appl. Bio Mater.* **2020**, *3*, 6439–6446. [[CrossRef](#)] [[PubMed](#)]

**Disclaimer/Publisher’s Note:** The statements, opinions and data contained in all publications are solely those of the individual author(s) and contributor(s) and not of MDPI and/or the editor(s). MDPI and/or the editor(s) disclaim responsibility for any injury to people or property resulting from any ideas, methods, instructions or products referred to in the content.